Optical-diffraction measurement of fractal dimensions and $f(\alpha)$ spectrum

J. F. Muzy and B. Pouligny
Centre de Recherche Paul Pascal, Avenue Schweitzer, 33600 Pessac, France

E. Freysz
Centre de Physique Moléculaire Optique et Hertzienne, Université de Bordeaux I, 33405 Talence CEDEX, France

F. Argoul and A. Arneodo
Centre de Recherche Paul Pascal, Avenue Schweitzer, 33600 Pessac, France

(Received 10 February 1992)

The optical-wavelet transform (OWT) is used to measure the generalized fractal dimensions D_q and the related $f(\alpha)$ spectrum of singularities of fractal aggregates. Its ability to characterize geometrical multifractality is demonstrated on deterministic fractals. Application of the OWT to experimental copper electrodeposition clusters in the limit of small ionic concentration and small voltage is reported. The statistical self-similarity of these experimental clusters and Witten and Sander diffusion-limited aggregates is confirmed.

PACS number(s): 64.60.Ak, 07.60.−j, 42.30.−d, 61.50.Cj

Most of the experimental determinations of the fractal dimension D of fractal structures are based on scattering experiments with x rays, neutrons, or light [1]. Widely used in the study of critical phenomena at phase transitions, these techniques provide a convenient experimental method of characterizing the geometrical scaling properties of fractal objects. Generally, D is extracted from the power-law behavior of the scattered intensity $I(k)\sim k^{-D}$, where k is the scattering wave vector. This scaling law indicates that the density-density correlation function behaves as $g(r)\sim r^{D-d}$, where d is the dimension of space. In the pioneering studies [1], this scaling analysis was mainly concerned with stochastic structures. More recently it has been generalized to deterministic fractals [2]. But, as emphasized in recent theoretical works [3,4], the estimate of the fractal dimension D does not provide a deep insight into the geometrical complexity of fractal objects. A better characterization would, for example, require measuring the scaling exponents D_n of higher-order correlation functions. These exponents are inaccessible to classical scattering techniques which are based on a simple Fourier transform. The aim of this Brief Report is to demonstrate that the double Fraunhofer diffraction experimental arrangement designed in a previous work [5] to perform the optical-wavelet transform (OWT) can be adapted to extract the generalized (to real values of q) fractal dimensions [3] D_q and the closely related $f(\alpha)$ spectrum of singularities [6]. We will mainly focus in this study on fractal aggregates in two dimensions. For homogeneous (globally self-similar) aggregates, the OWT reveals that the D_q's are all equal, i.e., their $f(\alpha)$ spectrum is concentrated on a single point $\alpha=D_0$. In this case, the two-point correlation dimension $D=D_2$ measured by classical scattering experiments is the actual fractal dimension D_0. For multifractals [6], D_2 is different from D_0, and D_q is generally a monotonously decreasing function of q, while the $f(\alpha)$ spectrum turns out to be a single-humped function of maximum D_0. For its ability to characterize geometrical multifractality, the OWT is a definite step beyond simple diffraction.

The wavelet transform (WT) has been the subject of considerable theoretical developments and practical applications in a wide variety of fields [7]. Of recent interest is the application of wavelets to fractals [4,8], e.g., fractal aggregates grown in a diffusion field [9]. In a previous study [5], we have shown that a very cheap and fast way to perform the WT consists in using coherent optical spatial-frequency filtering. The WT of a real function ρ over $\mathbb{R}^d$ (in practice, a mass density), with respect to an isotropic analyzing wavelet g, is given by the convolution product

$$T_g(a,\mathbf{x})=\left[\rho(\mathbf{x}')\otimes\frac{1}{a^d}g\left[\frac{\mathbf{x}'}{a}\right]\right]_{\mathbf{x}} . \tag{1}$$

$T_g(a,\mathbf{x})$ is the wavelet component of ρ for the length scale $a\,(>0)$. The analyzing wavelet g is just required to be continuous and of zero mean [7]. Fourier transforming Eq. (1) gives

$$\hat{T}_g(a,\mathbf{k})=\hat{\rho}(\mathbf{k})\hat{g}(a\mathbf{k}) , \tag{2}$$

where the caret denotes the Fourier transform. $\hat{g}$ has to be zero at $\mathbf{k}=0$ as the consequence of the requirement $\langle g\rangle=0$. Calculating the wavelet component of size a of ρ just amounts to filtering its Fourier-transform spectrum with a filter of transparency $\hat{g}(ak)$. In the OWT [5] the object ρ is Fourier transformed in a classical Fraunhofer diffraction geometry, with a lens of focal length f. The electromagnetic field distribution in the rear focal plane of the lens is proportional to $\hat{\rho}(\mathbf{k})$, with $\mathbf{k}=2\pi\mathbf{u}/\lambda f$; here $\mathbf{u}$ is the position in the Fourier plane and λ is the light source wavelength. The simplest acceptable filter shape to be used in the Fourier plane is a binary approximation of the Fourier transform of the sombrero (Mexican hat)

 ©1992 The American Physical Society

[9]: the filter transparency is equal to one for $R/\gamma < |\mathbf{u}| \leq R$, and zero elsewhere. This is just a bandpass filter that admits frequencies between $2\pi R/\lambda f\gamma$ and $2\pi R/\lambda f$. The filter is located in front of another lens which images the filtered sample, i.e., its wavelet component at scale $a=\lambda f/2\pi R$. The whole WT is completed by repeating this filtering for different values of a, in practice with homothetic bandpass filters [10].

Figure 1 sketches our current optical-wavelet transform setup. A complete description can be found in Ref. [10]. For the purpose of this Brief Report it suffices to know that the experiment uses a stack of 31 homothetic bandpass filters, whose dynamical range is equal to 27. The setup comprises two paths, corresponding to two different values of f. The resulting overall dynamical range is a bit more than two decades. The samples used up to now are large-size photographic slides that can accommodate up to 1024×1024 pixels. The filtered images are sent to a charge coupled device (CCD) camera which is coupled to a DEC 3200 workstation that can process and store the images at the video rate. Since the video camera is a quadratic detector, the OWT actually gives $I(a,\mathbf{x})=|T_g(a,\mathbf{x})|^2$.

In our preliminary study [5] we have pointed out the ability of the OWT to resolve local scaling properties of fractals. If the mass of a fractal aggregate scales around the point $\mathbf{x}_0$ with the scaling exponent $\alpha(\mathbf{x}_0)$

$$\mu(\mathcal{B}(\mathbf{x}_0,\lambda\epsilon))=\int_{\mathcal{B}(\mathbf{x}_0,\lambda\epsilon)}\rho(\mathbf{x})d\mathbf{x}\sim\lambda^{\alpha(\mathbf{x}_0)}\mu(\mathcal{B}(\mathbf{x}_0,\epsilon)) , \quad (3)$$

where $\mathcal{B}(\mathbf{x}_0,\epsilon)$ is an ϵ ball centered at $\mathbf{x}_0$, then the intensity recorded at this point on the CCD camera will behave like [5,10]

$$I(\lambda a,\mathbf{x}_0)=|T_g(\lambda a,\mathbf{x}_0)|^2\sim\lambda^{2[\alpha(\mathbf{x}_0)-2]}|T_g(a,\mathbf{x}_0)|^2 . \quad (4)$$

Now, in the spirit of the multifractal formalism [6], let us define a partition function in terms of the wavelet components [11],

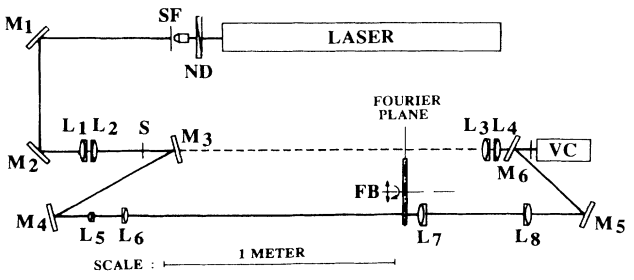

FIG. 1. Optical-wavelet transform setup. The light source is a krypton laser. The L_i's are doublet lenses and M_i's are mirrors. The filters are brought into operation in the Fourier plane by a robot. Path 1 (corresponding to small-scale wavelet components) is in operation when M_3 and M_6 are removed. The figure shows path 2 (large-scale components in operation). SF, spatial filter; ND, variable neutral density filter; S, sample; FB, bandpass filter barrel; VC, video camera.

$$Z(a,q)=\int d\mu(\mathbf{x})[a^2\sqrt{I(a,\mathbf{x})}]^{(q-1)}\sim a^{(q-1)D_q} . \quad (5)$$

$Z(a,q)$ is thus obtained by summing $[a^2\sqrt{I(a,\mathbf{x})}]^{(q-1)}$ for all points $\mathbf{x}$ belonging to the fractal set or aggregate; the way it depends on the filter size (in the limit $a\rightarrow0^+$) directly gives the so-called order-q generalized dimensions. The set of local exponents α and the related $f(\alpha)$ spectrum of singularities are generated through the "canonical" equations [12]:

$$\begin{aligned}\alpha(q)&=\frac{d[(q-1)D_q]}{dq}\\&=\lim_{a\rightarrow0^+}\frac{1}{\ln a}\int d\mu(\mathbf{x})\mathcal{I}_q(a,\mathbf{x})\ln[a^2\sqrt{I(a,\mathbf{x})}] ,\\ f(\alpha(q))&=\lim_{a\rightarrow0^+}\frac{1}{\ln a}\int d\mu(\mathbf{x})\mathcal{I}_q(a,\mathbf{x})\ln\mathcal{I}_q(a,\mathbf{x}) ,\end{aligned} \quad (6)$$

where $\mathcal{I}_q(a,\mathbf{x})=[a^2\sqrt{I(a,\mathbf{x})}]^{(q-1)}/Z(a,q)$. This definition can be obtained by simply deriving the partition function [9] $Z(a,q)$ with respect to q. Note that it allows us to determine the $f(\alpha)$ curve using $\log_2$-$\log_2$ plots for both $\alpha(q)$ and $f(\alpha(q))$ without neglecting logarithmic corrections [12] and without facing the difficulties encountered [9] when directly Legendre transforming [6] $\tau(q)=(q-1)D_q$.

In Fig. 2, we report the OWT measurement of the D_q and $f(\alpha)$ spectra of deterministic mathematical aggregates. The one-scale snowflake shown in Fig. 2(a) is commonly thought of as a paradigm for globally self-similar aggregates [9]. Its iterative construction rule can be considered as a deterministic model for aggregation. A straightforward calculation [9] yields $D_q=\ln5/\ln3$ for all q. Therefore, each point of the aggregate corresponds to a single scaling index $\alpha=\ln5/\ln3$, with the density $f(\alpha=\ln5/\ln3)=\ln5/\ln3$. The OWT measurement of the D_q's is shown in Fig. 2(c) where the partition function is plotted versus a in a log-log representation. The slope D_q of the graph obtained for a given q is reported in Fig. 2(d) as a function of q. The errors bars correspond to the fluctuations observed around the straight lines in the $\log_2$-$\log_2$ plots in Fig. 2(c). These fluctuations are the combination of finite-size effects and experimental noise superposed onto intrinsic periodic oscillations [9] of period $P=\ln3$. These oscillations are due to the invariance of the one-scale snowflake under dilation of length scales by the scale factor $l=3$. The OWT provides an accurate estimate of the D_q's: within the experimental uncertainty, the generalized fractal dimensions are all equal to the theoretical value $D_q=\ln5/\ln3$. This is an experimental checking of the capability of our experimental technique to recognize global self-similarity.

Figure 2(b) shows a two-scale snowflake [9] constructed at stage n by adding the configuration at the $(n-1)$th stage of the growth to the four corners of the twice-enlarged version (and not the same version as for the one-scale snowflake construction rule) of the cluster corresponding to the $(n-1)$th-stage configuration (the ratio of the two-scale factors $l_1/l_2=2$). Since the two-scale snowflake has an exact recursive structure, the generalized fractal dimensions D_q and the $f(\alpha)$ spectrum can be

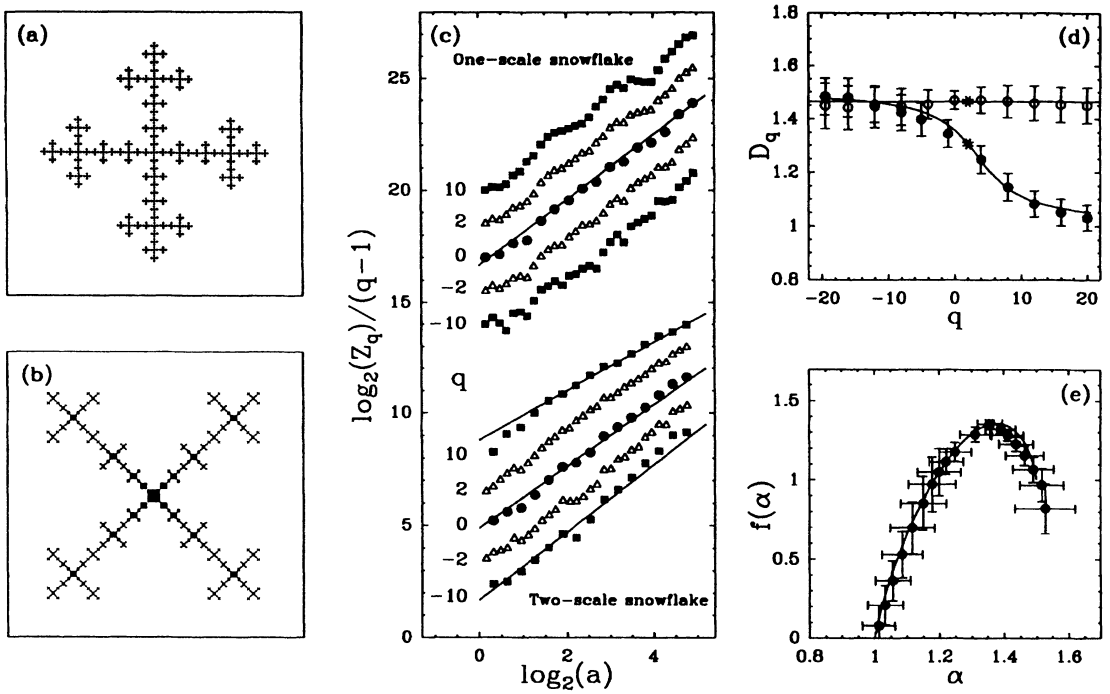

FIG. 2. OWT measurement of the D_q's and $f(\alpha)$ spectrum of the (a) one-scale and (b) two-scale snowflake fractals. The construction of each sample has been limited to six generations (see text). (c) $\mathrm{Log}_2 Z(a,q)/(q-1)$ vs $\log_2 a$ (arbitrary scales) for different values of q. (d) D_q vs q for the one-scale (○) and two-scale (●) snowflake; the symbol * corresponds to the two-point correlation dimension D_2, i.e., the only dimension accessible to classical scattering experiments. (e) The experimental $f(\alpha)$ spectrum of the two-scale snowflake. The solid lines in (c)–(e) correspond to the theoretical predictions (see text).

computed analytically [9]. These theoretical predictions (solid lines) are compared to our optical experimental measurements in Figs. 2(d) and 2(e), respectively. The data reveal a rather smooth decreasing dependence of D_q as a function of q. This evolution is visible in Fig. 2(c). The data for the corresponding $f(\alpha)$ spectrum are shown in Fig. 2(e). This spectrum is characteristic of multifractal objects [4,6]. The scaling exponent α is not unique; it is experimentally found in a finite range $\alpha_{\min} \leq \alpha \leq \alpha_{\max}$, where the bounds $\alpha_{\min}$ and $\alpha_{\max}$ are given by the strongest and weakest singularities, respectively. The lower bound $\alpha_{\min} = D_{+\infty} = 1$, $f(\alpha_{\min}) = 0$, corresponds to the central point, i.e., the region of highest mass, where the largest scale factor l_1 has been applied at each stage of construction [Fig. 2(b)]. Conversely, $\alpha_{\max} = D_{-\infty} = 1.5$ corresponds to the regions of lowest mass, where the smallest scale factor l_2 has been successively applied; these regions have a finite density exponent $f(\alpha_{\max}) = 1$. The actual fractal dimension of the two-scale snowflake is the value D_q for $q = 0$, which is also the maximum of the $f(\alpha)$ curve, $D_0 = 1.34 \pm 0.05$. This value is larger than the two-point correlation dimension $D_2 = 1.29 \pm 0.05$, usually identified to the fractal dimension in classical diffraction experiments [1,2]. The data shown in Figs. 2(d) and 2(e) are in remarkable agreement with the theoretical D_q and $f(\alpha)$ curves. Multifractality of the two-scale snowflake is thus demonstrated experimentally.

Among the various experimental illustrations of fractal pattern-forming phenomena, electrochemical deposition

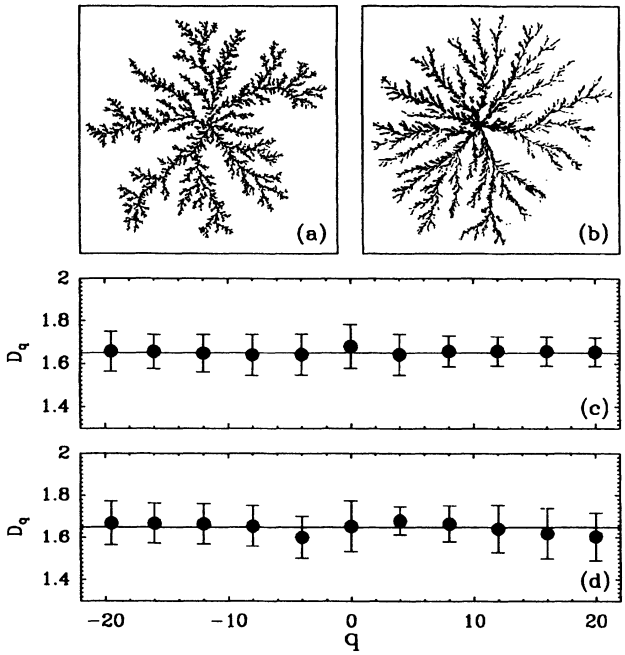

FIG. 3. (a) An off-lattice DLA cluster of mass $M = 50\,000$ (courtesy of P. Meakin) [19]. (b) An electrochemical fractal aggregate grown in circular geometry; the experimental conditions are defined in Ref. [9]. OWT determination of the D_q's of the (c) numerical DLA cluster and (d) experimental electrodeposit; the solid lines correspond to the mean-field prediction $D_F = \frac{5}{3}$.

[13] is commonly considered as the paradigm for theoretical studies of diffusion-limited aggregation. In fact, by varying the concentration of metal ions and the cathode potential, one can explore a rich variety of morphologies. Fractal patterns are usually obtained in the limit of small ionic concentration and small current density. These fractal electrodeposition clusters have been extensively studied [14] and it has been conjectured that they are similar to diffusion-limited aggregates (DLA) computed with the random walker model of Witten and Sander [15]. Only very recently the deep connection between highly ramified electrodeposits and DLA clusters has been established on a quantitative basis [9,16]. We show in Fig. 3 the OWT determination of the spectrum of generalized fractal dimensions of off-lattice DLA clusters [17] of mass $M=50\,000$ [Fig. 3(a)] and a fractal copper electrodeposition cluster grown in a circular geometry [Fig. 3(b)]. The data for the D_q's of these aggregates are reported in Figs. 3(c) and 3(d), respectively. The global self-similarity of these numerical and experimental aggregates is confirmed by our OWT analysis. The data do not reveal any significant deviation from a constant D_q curve. Moreover, the dimensions for the electrodeposition ($D_q=1.66\pm0.08$) and DLA ($D_q=1.65\pm0.06$) clusters are the same within the experimental uncertainty and in good agreement with recent numerical dimension measurements [9,16]. Note that our experimental data match the mean-field prediction [18] $D_F=\frac{5}{3}$ for diffusion-limited aggregation in $d=2$ dimension. The results in Fig. 3 provide the experimental demonstration that electrodeposition and DLA clusters are statistically self-similar and that their fractal properties, when characterized by such quantities as their generalized fractal dimensions, or the related $f(\alpha)$ spectrum, are identical.

In conclusion, we have shown that the optical-diffraction device, designed to perform analogically the WT, is a very powerful experimental tool that can resolve geometrical multifractality. Preliminary results of a study of Laplacian fractal growth phenomena show that the OWT can also be applied to characterize the multifractal properties of the velocity field along the cluster interface. For its ability to analyze the scaling behavior of high-order correlation functions, the OWT is a definite step beyond classical scattering techniques. Its application to revisit phase transitions in critical phenomena looks very promising. The study of critical colloidal systems is currently in progress.

We are very grateful to G. Gabriel and M. Vega for their technical assistance. This work was supported by the Région Aquitaine, the MEN under Contract No. DRED3-1322, the DRET under Contract No. DRET 89-196, and the CNES under Contract No. 90-CNES-215.

[1] J. Texeira, in *On Growth and Form: Fractal and Non-Fractal Patterns in Physics,* edited by H. E. Stanley and N. Ostrowsky (Nijhof, Dordrecht, 1986), p. 145; S. K. Sinha, Physica D **38**, 310, (1989), and references therein.

[2] C. Allain and M. Cloitre, Phys. Rev. B **33**, 3566 (1986).

[3] P. Grassberger and I. Procaccia, Physica D **13**, 34 (1984).

[4] A. Arneodo, F. Argoul, J. Elezgaray, and G. Grasseau, in *Nonlinear Dynamics,* edited by G. Turchetti (World Scientific, Singapore, 1988), p. 130.

[5] E. Freysz, B. Pouligny, F. Argoul, and A. Arneodo, Phys. Rev. Lett. **64**, 745 (1990).

[6] T. C. Halsey, M. H. Jensen, L. P. Kadanoff, I. Procaccia, and B. I. Shraiman, Phys. Rev. A **33**, 1141 (1986).

[7] *Wavelets,* edited by J. M. Combes, A. Grossmann, and P. Tchamitchian (Springer-Verlag, Berlin, 1989).

[8] A. Arneodo, G. Grasseau, and M. Holschneider, Phys. Rev. Lett. **61**, 2281 (1988); in *Wavelets* (Ref. [7]), p. 182; M. Holschneider, J. Stat. Phys. **50**, 963 (1988).

[9] F. Argoul, A. Arneodo, J. Elezgaray, G. Grasseau, and R. Murenzi, Phys. Lett. A **135**, 327 (1989); Phys. Rev. A **41**, 5537 (1990).

[10] B. Pouligny, G. Gabriel, J. F. Muzy, A. Arneodo, F. Argoul, and E. Freysz, J. Appl. Cryst. **24**, 526 (1991).

[11] J. F. Muzy, E. Bacry, and A. Arneodo, Phys. Rev. Lett. **67**, 3515 (1991).

[12] A. Chhabra, C. Meneveau, R. V. Jensen, and K. R. Sreenivasan, Phys. Rev. A **40**, 5284 (1989).

[13] L. M. Sander, in *The Physics of Structure Formation,* edited by W. Guttinger and G. Dangelmayr (Springer-Verlag, Berlin, 1987), p. 257.

[14] R. M. Brady and R. C. Ball, Nature **309**, 225 (1984); M. Matsushita, M. Sano, Y. Hayakawa, H. Honjo, and Y. Sawada, Phys. Rev. Lett. **53**, 286 (1984); D. G. Grier, E. Ben-Jacob, R. Clarke, and L. M. Sander, *ibid.* **56**, 1264 (1986).

[15] T. A. Witten and L. M. Sander, Phys. Rev. Lett. **47**, 1400 (1981); Phys. Rev. B **27**, 5686 (1983).

[16] F. Argoul, A. Arneodo, G. Grasseau, and H. L. Swinney, Phys. Rev. Lett. **61**, 2558 (1988).

[17] P. Meakin, J. Phys. A **18**, L661 (1985).

[18] M. Tokuyama and K. Kawasaki, Phys. Lett. **100A**, 337 (1984); K. Honda, H. Toyoki, and M. Matsushita, J. Phys. Soc. Jpn. **55**, 707 (1986).

[19] Reproduced from Ruskai *et al.* (ed), Wavelets and Their Applications, © 1992 Jones and Bartlett Publishers, Inc. All rights reserved. Reprinted with permission of the publisher.